Indian Journal of Chemical Technology
Vol. 33, July 2026, pp. 523-534
DOI: 10.56042/ijct.v33i4.30557

Oil industry waste derived activated carbon for malachite green dye adsorption: Kinetic, isotherm, and thermodynamic study

Ankita Sao & Mahendra S. Gaikwad*

Department of Chemical Engineering, National Institute of Technology Raipur, Raipur -492010, Chhattisgarh, India

*E-mail: mahendra14g@gmail.com/msgaikwad.che@nitrr.ac.in

Received 18 April 2026; accepted 23 July 2026

This study explores de-oiled rice bran (DORB), an agro-industrial by-product, as a precursor for the preparation of porous activated carbon. The study assesses the performance of the synthesized activated carbon (AC) in removing malachite green (MG) dye from aqueous solutions, with a focus on developing economically viable and sustainable adsorbents for wastewater treatment. AC was synthesized using a combined thermal and chemical modification process with H_3PO_4, eliminating the need for separate activation steps. This approach reduced preparation time and energy consumption. The resulting activated carbon possessed a surface area of 465 m^2 g^{-1} and an average pore size of 5.0872 nm. Characterization was performed using SEM, FTIR, EDAX, and pH_{pzc} techniques. The adsorption performance was studied under varying pH (3.0–9.0), initial MG concentration (10–50 mg L^{-1}), adsorbent dosage (0.1–0.6 g), contact time (0–30 min), and temperatures (303–333 K). The adsorption behaviour followed the Freundlich isotherm model, and the kinetics were well described by the pseudo-second-order model. The highest adsorption capacity was 70.92 mg g^{-1}. Thermodynamic analysis revealed spontaneous ($\Delta G<0$), endothermic ($\Delta H>0$), and favourable ($\Delta S>0$) adsorption. Regeneration studies identified 0.2 M HCl as an effective solvent for De-oiled rice bran activated carbon (DORBAC) recovery.

Keywords: Activated carbon, Adsorption isotherm, Agro-waste valorization, De-oiled rice bran, Malachite green, Wastewater treatment

Introduction

Rapid urbanization and the intensification of industrial operations have given rise to the most inescapable difficulties of the widespread exploitation of water resources, resulting in a scarcity of clean water [1]. In the past, people obtained colourants from roots, shells, flowers, mollusks, and insects. However, most colouring agents have been substituted by synthetic alternatives, as synthetic dyes can be produced on a big scale [2]. The textile industry releases a significant proportion of wastewater, reaching up to 900 million tons yearly, ranking it 6th in industrial discharge volumes [3]. Malachite green (MG) functions as a cationic dye in cotton, jute, silk, wool, acrylic, paper, and leather industries. It is a crucial component in fish farming and hatchery businesses, acting as a reliable antiparasitic, antimicrobial, and antifungal agent [4]. Along with that it finds application in food pigments, preservatives, germicides, and antiparasitic agents [4–6].

The environmental persistence of MG dye causes serious toxic effects, including eye burns, rapid breathing, excessive sweating, cancer, and damage to the brain, nervous system, and liver. It also reduces food intake and impairs growth and fertility[7,8,9]. It can adversely affect multiple organs, including the heart, liver, and kidneys. It can result in skin, eye, lung, and bone issues. Additionally, it can lead to congenital abnormalities and harm animal cells. MG can lead to dyscrasia, anemia, leukocytosis, and blood coagulation delay. It disrupts photosynthesis in the hydrosphere by blocking light from penetrating and has a deleterious influence on aquatic life [2,7,8]. Although banned in many countries and not approved by the U.S. Environmental Protection Agency for aquatic use, MG dye is still widely used because it is inexpensive, readily available, and highly effective [9,10].

Even if new carbon compounds like graphene, carbon aerogel, and carbon nanotubes have gained popularity [11]. Activated carbon (AC) remains a practical choice for various applications, including eliminating pollutants, storing energy, catalysts, and gas capture, due to its straightforward synthesis process and abundant availability [12,13]. Commercial activated carbon (CAC) is frequently employed to

eliminate dyes owing to their characteristics, including porosity, extensive surface area, and higher adsorption capacity. However, a major limitation of commercial activated carbon is its significant cost and the difficulties associated with regeneration [14]. One potential solution to these problems involves the development of AC made from various biomass including straws, shells, agricultural and industrial by-products, and residues [15]. Inexpensive or minimally valued as materials, these biomass-based raw materials can be effectively utilized to synthesize activated carbon. Additionally, this may address the issue of waste disposal [16].

De-oiled rice bran (DORB) is the agriculture-based industrial byproduct remaining after rice bran oil extraction, which is considered waste and used as animal feed. Studies have reported that feeding higher levels of DORB can cause stress to fish breeds like Labeorohita[17]. However, it is capable of being transformed into a highly potent adsorbent. Several research studies have explored the possibility of using low-cost agro-industrial by-products to remove MG dye from aqueous solutions efficiently. These include peanut hull [18], banana stem [19], etc. Although DORB has been explored as a low-cost precursor for adsorbent production, studies on its application for dye removal remain limited, and most have relied on conventional multi-step activation methods. To the best of our knowledge, the use of a single-step thermo-chemical activation process employing H_3PO_4 specifically for DORB has not been systematically investigated for MG dye adsorption. This integrated activation approach combines carbonization and chemical activation into a single process, reducing processing time and energy consumption while generating a highly porous adsorbent, thereby providing a simple, cost-effective, and sustainable strategy for producing efficient adsorbents from DORB.

Experimental Section

Materials and preparation

The chemicals utilized in this work include MG dye ($C_{53}H_{54}N_4O_{12}$; molecular weight 927 g mol^{-1}; λ_{max}=616 nm), procured from Loba Chemie Pvt. Ltd. Phosphoric acid (H_3PO_4) was utilized for chemical activation, while NaOH and HCl were employed for pH adjustment. All reagents were of analytical grade and procured from Loba Chemie Pvt. Ltd. Working solutions of MG (10–50 mg L^{-1}) were formulated by dilution a 1000 mg L^{-1} stock solution.

DORB residue was obtained from a nearby marketplace in Raipur, Chhattisgarh. Distilled water was employed to clean the DORB residue thoroughly. Subsequently, the residual moisture in DORB was eliminated by dehydrating overnight. The dehydrated residue was broken down employing a mortar and pestle and filtered through a 100 µm sieve.

The one-step method is chosen for activation because it is more effective in energy and relative time than the traditional two-step activation process. The impregnation of DORB with H_3PO_4 is done in 20% (w/w) thoroughly mixed and treated in a muffle furnace under an ambient atmosphere with 8 ℃ min^{-1} ramp rate from ambient to 400 ℃ for four hours. The resulting material was allowed to cool and removed at ambient temperature. To eliminate any chemical residue, the final substance was thoroughly rinsed repeatedly with distilled water until its pH matched that of the distilled water, continued by drying at 80℃ and grinding. The significant advantages of using one-step activation are that it is less energy and time-intensive, and the complete synthesis in air ambient omits the requirement of sophisticated equipment [20]. The final product, de-oiled rice bran-based activated carbon using one-step activation is further utilized in studies and has been characterized using the following equipment. The thermal stability of raw DORB is assessed using the Setaram Labsys Evo Thermogravimetric analyzer. Functional moieties present on the synthesized de-oiled rice bran activated carbon (DORBAC) were verified using FTIR spectroscopy with a Bruker Alpha Model spectrophotometer. The surface topography of DORBAC was characterized using the ZEISS EVO Series Scanning Electron Microscope Model EVO 18. The elemental composition was ascertained using an energy-dispersive X-ray system, namely the INCA 250 EDS with an X-MAX 20 mm Detector. The Brunauer-Emmett-Teller surface area and Barrett-Joyner-Halenda (BJH) pore size distribution are determined using the BELSORP-max II instrument from Microtrac BEL Corp. The point of zero charge (pH_{pzc}) was found out by the Litesizer-500, Anton Paar Zeta Potential Analyzer.

Batch experiment

Different amounts of DORBAC were supplemented to 50 mL of MG dye at ambient temperature, with magnetic agitation at pH 9 to estimate the amount of MG adsorbed. The absorbance disparities were calculated by UV-visible (Shimadzu, UV-1800) at a

peak wavelength (λ_{max}=616 nm) at altered periods of (3, 6, 9, 12, 15, and 18 min) through the adsorption method to explore the impact of contact duration. The decision to choose λ_{max} was based on the maximum absorbance observed for the adsorbate during spectrophotometric analysis conducted amidst the wavelength spectrum of 200 nm to 800 nm, using distilled water as the reference standard. The impact of the initial concentration of MG was evaluated from 10 to 50 mg L^{-1} for 18 min. The effect on the quantity of adsorbent used was estimated for various DORBAC concentrations (0.1 to 0.6 gL^{-1}) in 10 mg L^{-1} of MG solution. The equations used to calculate removal efficiency and adsorption capacity (q) can be expressed as follows in Eq. (1) and Eq. (2):

$$\% \, Removal = \frac{C_o - C_e}{C_o} \times 100 \quad \ldots (1)$$

$$q = \frac{(C_o - C_t)\, V}{m} \quad \ldots (2)$$

Where, C_o represents the initial concentration of MG and C_t signifies the concentration of remaining MG (mg L^{-1}), while V (L) is the volume of MG dye used, and m (g) is the quantity of DORBAC adsorbent employed in the experiment.

Methods

The kinetic models determine the duration needed to achieve equilibrium and the adsorption rate of the adsorbate. The adsorption technique was verified by selecting pseudo first order (PFO) and pseudo second order (PSO) models for this investigation.

The kinetic model proposed by Lagergren, also known as the PFO model, depicts the physisorption process that can be articulated as in Eq. (3):

$$\ln(q_e - q_t) = \ln q_e - k_1 t \quad \ldots (3)$$

Where, q_e: Quantity of MG adsorbed at equilibrium (mg g^{-1}), q_t: Quantity of MG adsorbed at time t (mg g^{-1}), k_1: PFO rate constant (min^{-1}) and t: Time (min).

The kinetic model proposed by Ho and McKay, also defined as the PSO model, depicts the chemisorption process, which can be expressed in Eq. (4):

$$\frac{t}{q_t} = \frac{1}{k_2 q_e^2} + \frac{1}{q_e} t \quad \ldots (4)$$

Where, k_2: PSO rate constant (g mg^{-1} min^{-1}).

The Freundlich and Langmuir isotherms were employed to understand better how uptake capacity correlates with MG concentration [21,22]. These two isotherms were explicitly chosen for their versatility in accurately representing a broad spectrum of adsorbate concentrations sorption process of MG onto DORBAC. The primary difference between the models is in the supposition, form of isotherm, and nature of the adsorbent. Langmuir model can be articulated in linear configuration as in Eq. (5) [23]:

$$\frac{C_e}{q_e} = \frac{1}{K_L q_m} + \frac{C_e}{q_m} \quad \ldots (5)$$

Where, C_e: Equilibrium dye concentration (mg L^{-1}), q_m: Highest adsorption capacity (mg L^{-1}) and K_L: Langmuir equilibrium constant (L mg^{-1}).

Langmuir isotherm model (LIM) is centered on the presumption of monolayer adsorption, occurring at specified homogeneous regions at the outer surface of the adsorbent, where additional adsorption is hindered once the adsorbate engages a site. The aspect crucially indicating conformity to the Langmuir model is the dimensionless separation factor (R_L) [24]. It can be expressed as given Eq. (6) [25]:

$$R_L = \frac{1}{1 + C_0 K_L} \quad \ldots (6)$$

Where, maximum initial dye concentration is denoted by C_0 (mg L^{-1}), and R_L demonstrates if Langmuir isotherm is either favourable ($0<R_L<1$), unfavourable ($R_L>1$), linear ($R_L=1$), or irreversible ($R_L=0$).

The Freundlich isotherm model (FIM) considers the translation of multi-faceted inclusion, where adsorption continues over the saturated adsorbent surface. Adsorption on uneven boundaries with consistent energy dissemination and revertible interaction is supported [26]. The heterogeneity factor (1/n) indicates the favourability and degree of adsorption, a smaller 1/n value (but greater than zero) recommends favourable adsorption behaviour and the adsorbent surface is heterogeneous with varying adsorption sites of varying affinities for the adsorbate.

The Freundlich isotherm in its linear form is expressed as in Eq. (7) [13]:

$$log q_e = \frac{1}{n} log C_e + log K_F \quad \ldots (7)$$

Where, 1/n: Heterogeneity factor and K_F: Freundlich equilibrium constant (L mg^{-1}).

The thermodynamic variables, including Gibbs free energy (ΔG), change in enthalpy (ΔH) and change in entropy (ΔS), were computed by surveying the

adsorption cycle at three modified temperatures (303K, 318K, and 333K) using van't Hoff equation was employed to calculate these factors mentioned below.

$$\Delta G = -RT\ lnK \quad \ldots (8)$$

$$K_d = \frac{q_e}{C_e} \quad \ldots (9)$$

$$\Delta G = \Delta H - T\Delta S \quad \ldots (10)$$

The equation below is derived by substituting Eq. (8) into Eq. (10). Eq. (9) is employed to calculate the adsorption distribution coefficient.

Where, T: Temperature (K), q_e: Equilibrium adsorption capacity (mg g^{-1}), R: Gas constant (8.314 J $mol^{-1}K^{-1}$), K_d: Adsorption distribution coefficient, C_e: Equilibrium dye concentration (mg L^{-1}).

Results and Discussion

Adsorbent characterization

The TGA analysis of DORB shown in Fig. 1(a) depicts stages of mass loss for temperatures up to 200°C, eliminating moisture. Between (200°C-600°C), the breakdown of organic components with a significant mass loss (~80%) and the breakdown of a more stable structure are observed in the 600-1000°C range.

The FTIR spectra display functional groups in the raw material, DORBAC, and MG dye-loaded DORBAC surface. The raw DORB spectra unveiled the diverse functional groups identified on the surface; the wide band at 3380 cm^{-1} corresponded to the hydroxyl group's O–H bond[27]. The observed maximum at 2928 cm^{-1} could be due to the elongation of C-H bonds in alkanes [28] and the maximum at 1651 cm^{-1} could be due to the stretching of the C=O bond [29,30]. In the pattern region (1500 to 500 cm^{-1}), a minor peak at 1526 cm^{-1} conforms to N-O stretching of nitro compounds; the band observed at 1379 cm^{-1} in the spectra is consistent with the symmetrical deformation of the CH_3 group [31], the peak noted at 1033 cm^{-1} was linked to the stretching vibration of the C–O–C bond [32], bands at 852 cm^{-1} might relates to C–H groups of aromatic ring vibration or to ethanol [33].

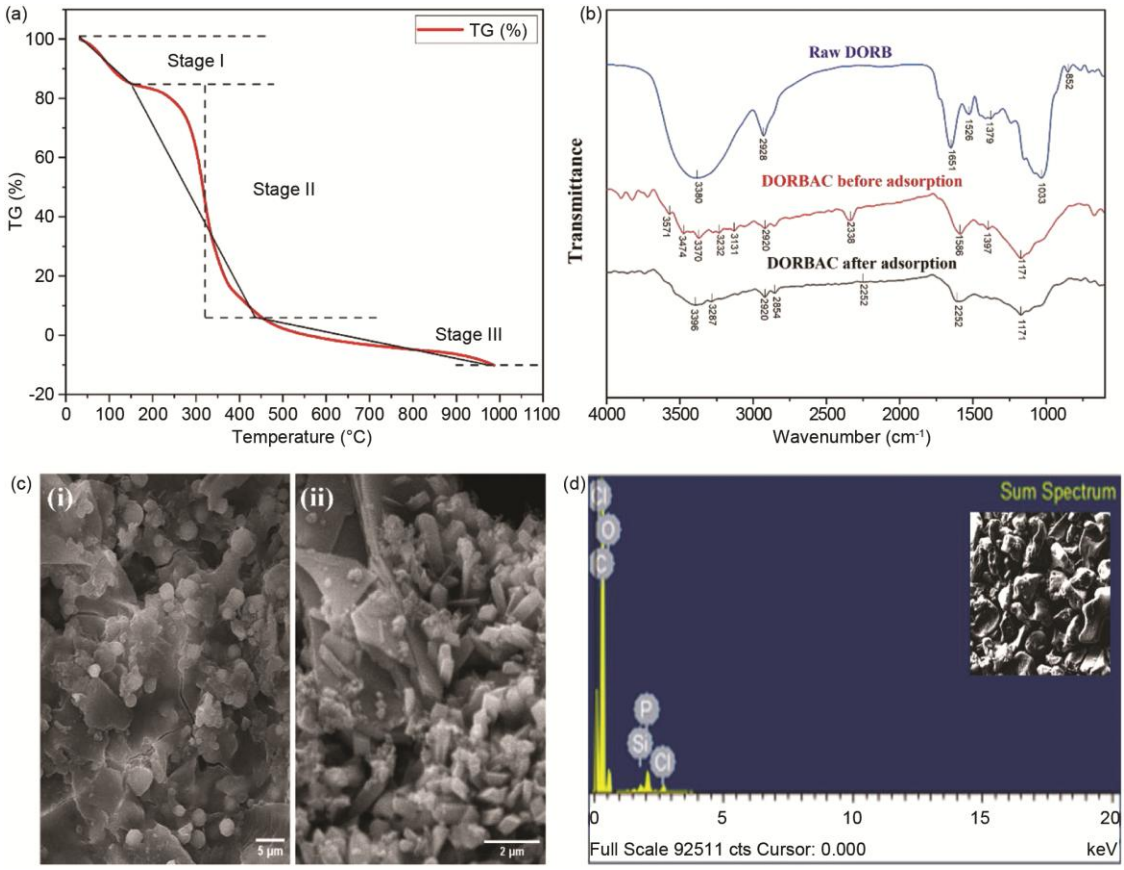

Fig. 1 — (a) Thermogravimetric curve for the combustion procedure of raw DORB, (b) FTIR spectra of raw DORBAC, before adsorption and after adsorption (c) SEM images of [(i) raw DORB and (ii) DORBAC] and (d) SEM-EDX images of DORBAC

After carbonization, the IR spectra changed significantly and different peaks appeared. A band of peaks appeared between 3200 cm^{-1} and 3700 cm^{-1} (3571cm^{-1}, 3474 cm^{-1}, 3370 cm^{-1}) shows OH carboxylic acid [27], a band of the peak near 3200 cm^{-1} (3232 cm^{-1}, 3131 cm^{-1}) may correspond to –NH stretching [13], at 2920 cm^{-1}, the stretching of the asymmetric CH_3 group's C–H bonds are observed [34], the band at 2338 cm^{-1} is attribute of the asymmetric stretching of physically adsorbed CO_2[35], peak observed at 1586 cm^{-1} corresponds to stretching vibrations of the C=C bonds in the aromatic ring [36], a weak peak at 1397 cm^{-1} can be due to N–H plane vibration [37], a sharp peak at 1171 cm^{-1} may correspond to S=O stretching of sulfonamide.[38]

In FTIR spectra Fig. 1(b), after MG adsorption, peaks of –OH 3571 cm^{-1}, –OH 3474 cm^{-1}, –NH 3131 cm^{-1}, and N–H 1397 cm^{-1} have disappeared, and few of the observed peaks were shifted to a higher wavenumber (3370 cm^{-1} to 3396 cm^{-1}, 3232 cm^{-1} to 3287 cm^{-1}, 2238 cm^{-1} to 2252 cm^{-1}, 1586 cm^{-1} to 1603 cm^{-1}). The phenomenon can be ascribed to establishing chemically bonded structures across the adsorbent–adsorbate interface, which might lead to new peaks or changes in existing peaks towards higher wavenumber.

Scanning electron microscopy (SEM) revealed the microstructure analysis of the synthesized DORBAC sample from raw DORB. The contrast in microstructural composition and shape of raw DORB and synthesized adsorbent is shown in Fig. 1(c). The micrographs show significant transformations in the physical microstructure of raw DORB and DORBAC. The raw DORB surface displays numerous delicate sheets or layers within its structure [39]. In contrast, DORBAC surface shows a highly rough, fractured, and irregular morphology, characterized by the development of numerous cavities, voids, cracks, and interconnected pores. The formation of these micro- and mesoporous structures significantly promotes an increase in specific surface area and pore accessibility, leading to the formation of abundant active sites for dye molecule interaction.

SEM-EDX analysis, shown in Fig. 1(d), indicates a significant increase in carbon levels compared to the raw DORB after the activation process (Tables 1 and 2**)**. The 2.98 wt% of potassium in the raw DORB vanished due to activated carbon production, as illustrated in Table 2. The rise in phosphorus in raw DORB to DORBAC of 2.99 wt% could be due to the use of phosphoric acid during activation [40]. The minute quantity of chlorine may be a by-product of chemical dust or impurity. Substances, predominantly consisting of carbon and oxygen, can efficiently eliminate dyes, heavy metals, and organic contaminants from aqueous systems[41]. Fig. 2(a) shows the elemental mapping of different elements present in DORBAC.

Table 1 — EDX findings for raw DORB

Element	Wt%	At%
C K	20.75	27.10
O K	68.89	67.56
Mg K	2.32	1.50
Si K	1.47	0.82
P K	3.60	1.82
K K	2.98	1.20
Total	100.00	100.00

Table 2 — EDX findings for DORBAC

Element	Wt%	At%
C K	47.72	57.35
O K	42.01	37.90
Si K	1.65	0.85
P K	6.59	3.07
Cl K	2.03	0.83
Total	100.00	100.00

Table 3 — Pore characteristics of DORBAC

Parameter	Value
S_{BET} (m^2 g^{-1})	465
V_t (cm^3 g^{-1})	0.7321
Average D_p (nm)	5.0872

S_{BET}, BET surface area; V_t, total pore volume; D_p, average pore diameter

A comprehensive evaluation of the porous framework of the synthesized DORBAC is done by utilizing the nitrogen adsorption-desorption isotherm. The results obtained are given in Table 3 show that the porous texture developed in DORBAC has an S_{BET} of 465 m^2 g^{-1} and a pore volume of 0.7321 cm^3 g^{-1}. Fig. 2(b) presents the N_2 adsorption isotherms of DORBAC. Based on the isotherm shape, DORBAC exhibited type II adsorption isotherms exhibit multilayer adsorption[42], as defined by the Brunauer, Deming, Deming, and Teller (BDDT) classification system. Fig. 2(c) shows the Barrett-Joyner-Halenda (BJH) pore size distribution graph with an average pore diameter of 5.0872 nm.

The pH_{pzc} of 2.46 mV was determined by mapping the zeta potential against the pH value. Fig. 2(d) illustrates how the zeta potential DORBAC varies with pH. With increased pH, the surface gains a more significant negative charge, boosting the likelihood of dye adsorption[43]. The highest negative charge of 36.5 mV was recorded at pH 9.

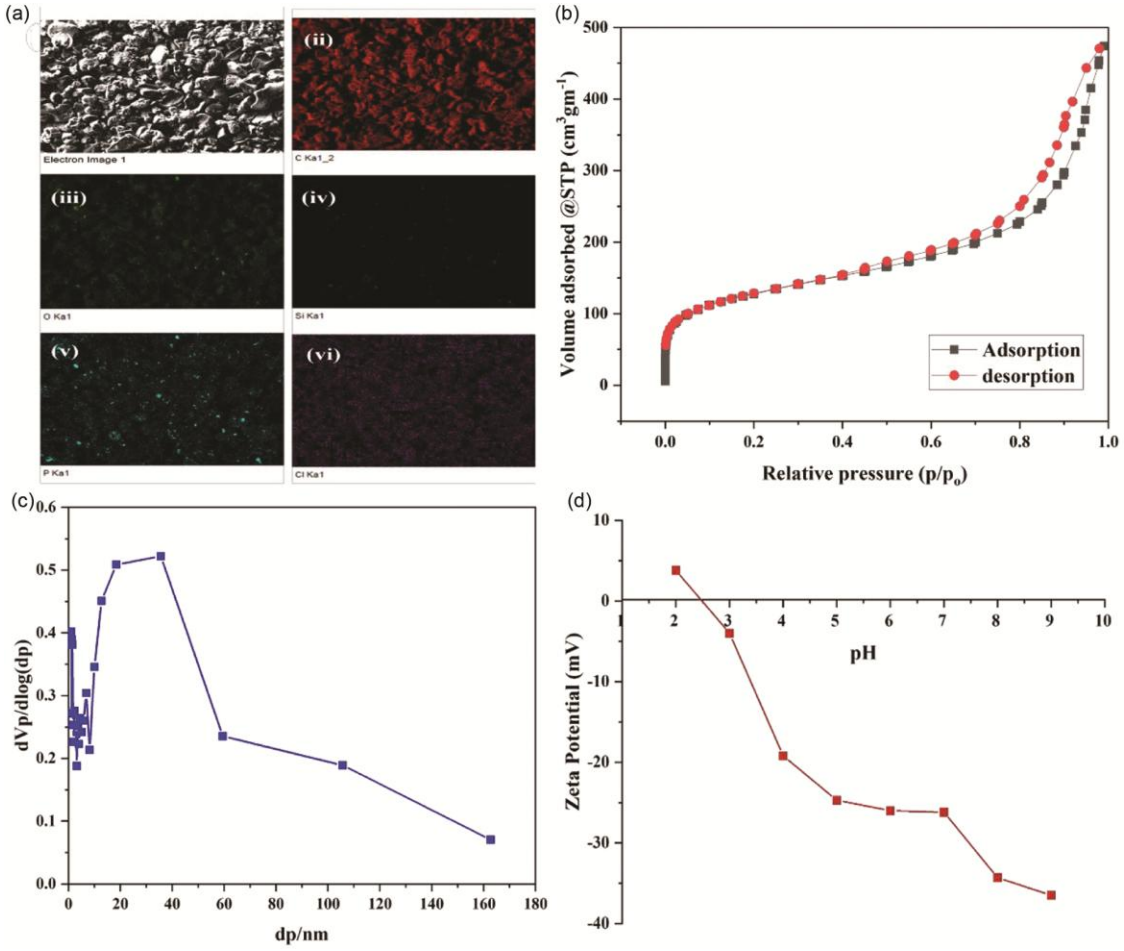

Fig. 2 — Structural and surface characterization of DORBAC (a) SEM–EDX elemental mapping, (b) N_2 adsorption–desorption isotherms at 77 K, (c) BJH pore size distribution, and (d) zeta potential as a function of pH for determination of the point of zero charge (pH_{pzc})

Batch adsorption studies

The pH strongly affects the colour intensity of MG and consequently affects its structural stability. Malachite green remained stable in the pH range of 3-10, thus the influence of initial pH was investigated over the pH range of 3-10 with an initial dye concentration of 10 mg L^{-1} (50 mL) and dosage of 0.4 g, as shown in Fig. 3(a). At the acidic region (pH=3) the removal efficiency is 82.25% whereas in the alkaline region (pH=9) is 99.85% after that removal efficiency slightly decreased. With increasing pH, the concentration of H^+ ions decreases, and the functional moieties present on the activated carbon surface (such as –OH and –COOH) become deprotonated, generating a negatively charged surface. This negative surface enhances electrostatic interaction between the adsorbent and the positively charged MG^+ dye molecules, leading to an increase in adsorption efficiency. Thus, pH 9 is considered optimum for all further experiments.

A sequence of investigations was executed to inspect the impact of varying adsorbent dosages; the dosage of the adsorbent was altered within the interval of 0.1 to 0.6 g L^{-1}, at MG dye concentration of 10 mg L^{-1}, pH 9 as shown in Fig. 3(b). The influence of adsorbent dosage was analyzed over the range of 0.1–0.6 g L^{-1} at an initial MG concentration of 10 mg L^{-1} and pH 9. The percentage removal efficiency increased from 71.79% to 99.91% as the dosage increased, owing to the greater availability of active adsorption sites and the specific surface area. However, beyond 0.4 g L^{-1}, the rise in adsorption efficiency became negligible due to possible agglomeration of adsorbent particles and saturation of available dye molecules. Therefore, 0.4 g L^{-1} was selected as the optimal adsorbent dose for further analysis.

The impact of initial concentration of 10-50 mg L^{-1} with a dosage of 0.4 g L^{-1}, pH=9. As illustrated in Fig. 3(c), the proportion of MG elimination minimizes

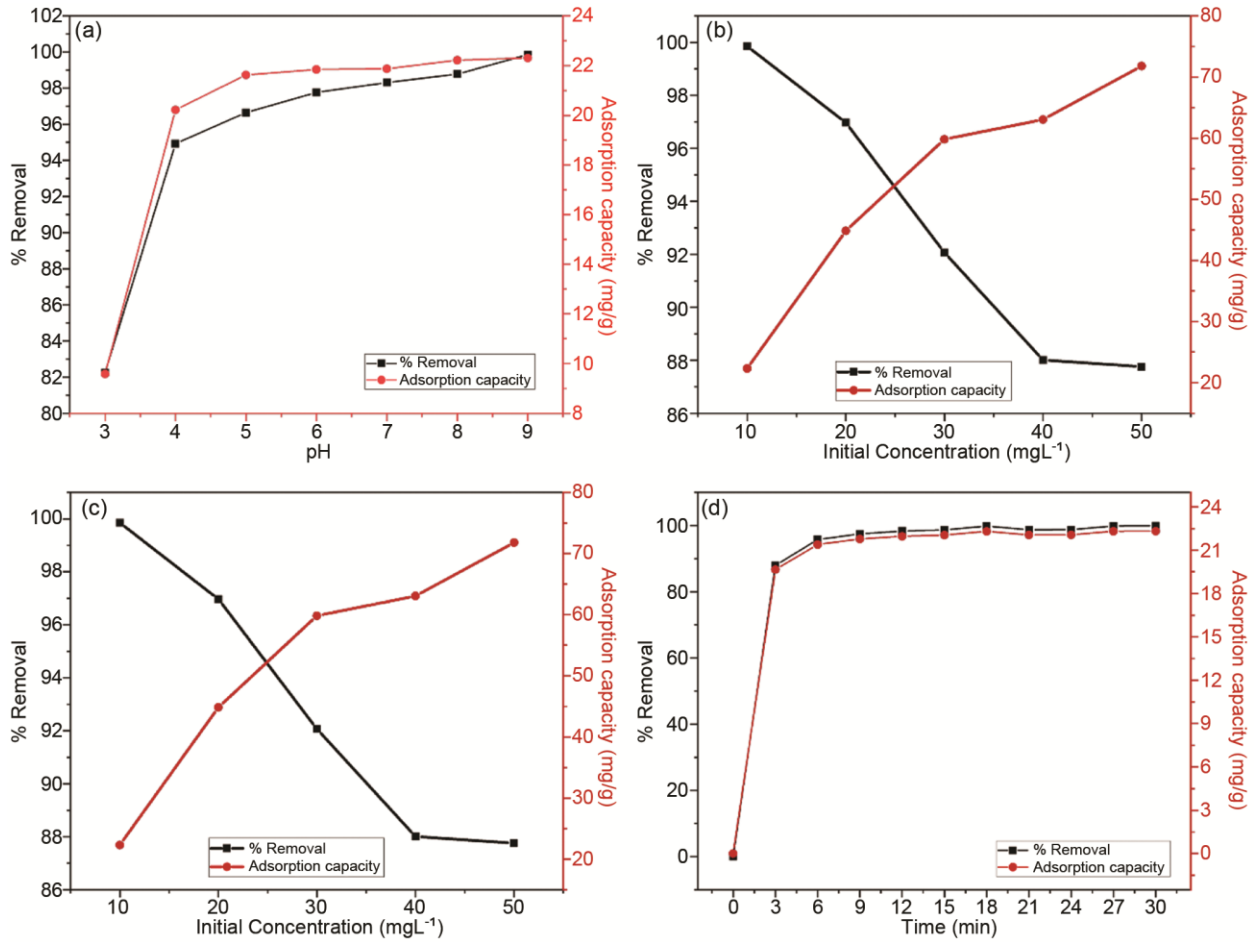

Fig. 3 — Effect of operational parameters on MG adsorption onto DORBAC: (a) solution pH, (b) adsorbent dosage, (c) initial dye concentration, and (d) contact time. Experimental conditions: initial MG concentration 10 mg L^{-1}, adsorbent dosage 0.4 g L^{-1}, pH 9, agitation speed 300 rpm, and room temperature

as the level of initial MG concentration increases. As the initial concentration increased from 10 to 50 mg L^{-1}, the adsorption capacity rose from 22.31 to 71.81 mg g^{-1}. Higher concentrations of the dye correspond to greater adsorption capacity (q_e). Adsorbents tend to have a higher dye uptake capacity when exposed to higher initial dye concentrations because of the enhanced abundance of dye species. This increases the overall interaction amid the adsorbent and the adsorbate[44].

The significance of the contact interval was examined across different time intervals (3-30 min) with a constant dosage of 0.4 g L^{-1}, pH=9, and initial concentration of 10 mg L^{-1}, as shown in Fig. 3(d). Numerous unoccupied sites and pores associated with the adsorbent material contribute to the swift initial adsorption. After all the active sites are filled, adsorption slows down. Eventually, the system reaches equilibrium and has the highest adsorption capacity. At an 18min contact interval, the removal efficiency hit a plateau, suggesting that equilibrium was finally attained[45]. Similar kinds of observations have been noted by Dahri *et al.*[22].

Adsorption kinetics

Kinetic curves withdraw evidence regarding the adsorption rate and the requisite duration to achieve equilibrium. In the PFO kinetics depicted in Fig. 4(a), the rate constant k_1 decreases with increasing dye concentration, indicating reduced adsorption rates at higher concentrations. The values for (q_e) are considerably lower than the experimental (q_{exp}) indicating a poor fit. In contrast, the PSO model is substantially closely matching the experimental evaluation, indicating a better fit, as shown in Fig. 4(b). The rate constant for both models decreases as the MG dye concentration increases, suggesting a decrease in adsorption rate as there is an increase in concentration attributable to the saturation of adsorption sites.

In addition, the correlation factor (R^2) found over the PSO model surpasses the PFO model in all cases. This implies that the experimental data was in great arrangement with PSO kinetics, as shown in Table 4. The adsorption mechanism is suggested to be chemisorption.

Adsorption isotherm

The isotherm curves for the Langmuir isotherm were drawn between C_e/q_e and C_e. For the Freundlich isotherm, they were drawn between log q_e and log C_e. Fig. 4(c) and (d) show the corresponding graphs of linear models of the isotherm and experimental data at different initial MG concentrations. Aiming to select the isotherm model, which superlatively characterizes the experimental data, evaluations were centered on the R^2 value. Freundlich has the maximum value compared to Langmuir, indicating that the FIM provided a better fit than the LIM. As presented in

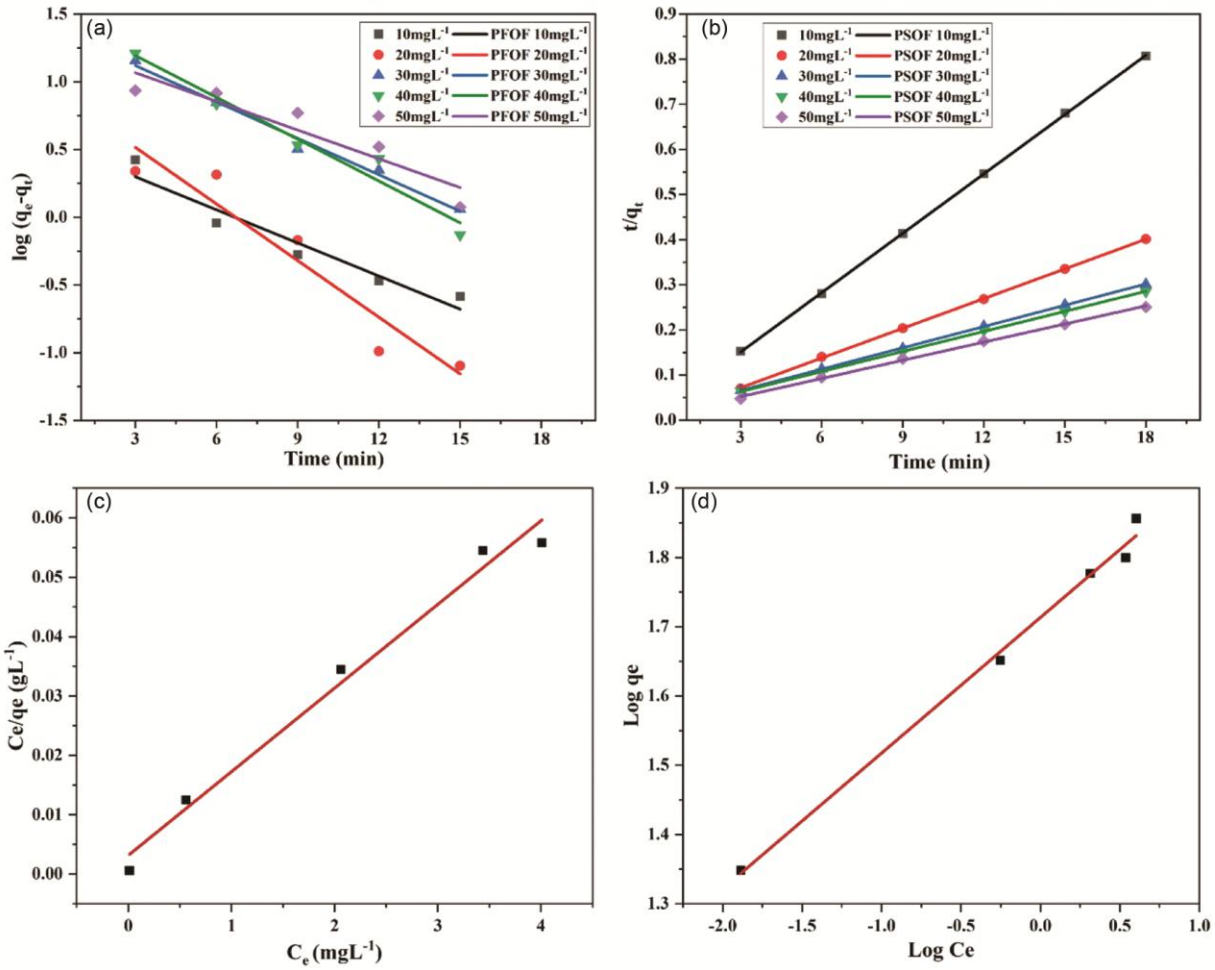

Fig. 4 — Adsorption kinetics and isotherm models for MG adsorption onto DORBAC: (a) PFO kinetic model, (b) PSO kinetic model, (c) Langmuir isotherm model (LIM), and (d) Freundlich isotherm model (FIM). Experimental conditions: adsorbent dosage 0.4 g L^{-1}, pH 9, agitation speed 300 rpm, contact time 18 min, and room temperature. Initial MG concentration ranged from 10–50 mg L^{-1}

Table 4 — Parameter values for PFO and PSO kinetic models at room temperature at different concentrations

Malachite green concentration	q_{exp}	Pseudo first order			Pseudo second order		
(mg L^{-1})	(mg g^{-1})	k_1 (min^{-1})	q_e(mg g^{-1})	R^2	k_2(g mg^{-1} min^{-1})	q_e (mg g^{-1})	R^2
10	22.31	-0.02714	3.493333	0.9121	0.098505	22.80502	0.9999
20	44.85	-0.02322	8.584006	0.8834	0.079172	45.57885	0.9998
30	59.83	-0.00996	24.49007	0.9837	0.013124	63.61323	0.9998
40	63.06	-0.00858	31.79582	0.9474	0.011676	67.47638	0.9997
50	71.81	-0.00471	19.01341	0.8286	0.015074	74.57122	0.9976

Table 5, the q_m of DORBAC foreseen through the LIM is 70.92 $mg^{-1}g^{-1}$. Although the Langmuir model predicts a q_{max} value, that differs from the measured q value by 0.89 units. The Freundlich model does not yield a singular q_{max} prediction but instead provides a spectrum of values that fluctuate with concentration, owing to its empirical character. Based on the extent of agreement to the experimental q value and the R^2 values, it can be concluded that the FIM provides a more accurate match to the experimental data[46]. A smaller value of heterogeneity factor (1/n) indicates a greater adsorption intensity and reflects the ease with which adsorbate molecules are adsorbed onto the adsorbent. The value of R_L lies within the extent of 0 to 1, which suggests that the MG uptake within the DORBAC adsorbent was favourable [47], as mentioned in Table 6.

Thermodynamic investigations

The investigation elucidates the effects of change in temperature on adsorption capacity and mechanism, and experimental observations indicate that an escalation in temperature caused a moderate increase in q_e, as shown in Table 4. It is stated that the van't Hoff equation fitted best with an R^2 value of 0.998, shown in Fig. 5. The adsorption is more favourable as ΔG decreases further into the negative range[48]. Most physical adsorption processes release heat, while chemisorption can exhibit either endothermic or exothermic nature. The values of ΔS and ΔH were determined from the intercept and slope of the plot of ln (K_d) versus 1/T, respectively, where K_d is calculated as the ratio of q_e to C_e. In contrast, Gibbs free energy is directly determined, ΔH and ΔS values were 15.85646 kJ mol^{-1} and 114.3009 kJ $mol^{-1}K^{-1}$, respectively, as given in Table 7. A positive ΔH signifies the endothermic nature of the adsorption [49]. A positive ΔS suggests affinity amongst MG and DORBAC and increases randomness amongst the dye species. Parallel outcomes have been articulated for MG adsorption on activated carbon by Chouli *et al*.[50]. Assessment of the maximum adsorption capacity of MG dye on different adsorbents is given in Table 8.

Table 5 — Langmuir isotherm model (LIM) and Freundlich isotherm model (FIM) statistical variables at varied MG concentrations for the adsorption of MG dye adsorption by DORBAC

Langmuir	q_m	K_L	R^2
	70.9219	0.2234	0.9793
Freundlich	K_F	1/n	R^2
	51.6951	0.1958	0.9931

Reusability studies

Industries are still dealing with the issue of disposing of spent adsorbent. Any adsorbent must acquire sufficient reusable characteristics to make the adsorption process more cost-effective and the reliance on an uninterrupted supply of adsorbent [58]. The reusability of the chemically regenerated adsorbent was assessed over five consecutive cycles. To achieve this, various desorption agents, such as distilled water, acetone, ethanol, and HCl, were applied. Fig. 6(a) shows that only 13.07% and 14.90% are desorbed using pure ethanol and acetone. In acidic

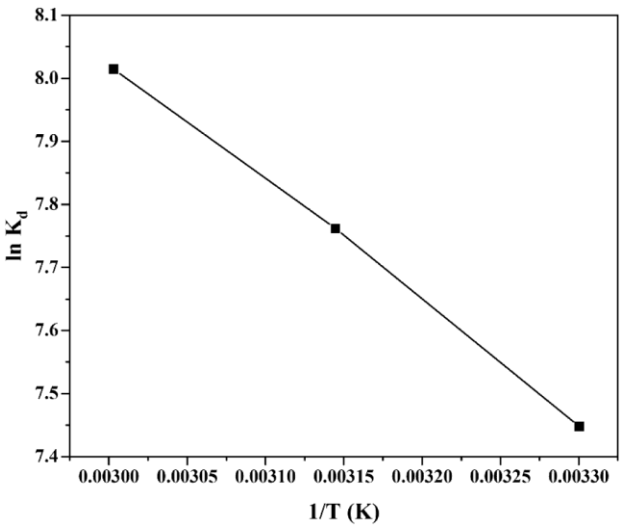

Fig. 5 — van't Hoff plot illustrating the temperature dependence of MG adsorption onto DORBAC

Table 6 — Value of R_L at varied MG concentration

Adsorbent	R_L values				
Concentration (mgL^{-1})	10	20	30	40	50
DORBAC	0.3092	0.1828	0.1298	0.1006	0.0821

Table 7 — Values of thermodynamic factors of MG adsorption on DORBAC at varied temperatures

T (K)	ΔG (kJ mol^{-1})	ΔH (kJ mol^{-1})	ΔS (kJ mol^{-1} K^{-1})	q_e (mg g^{-1})
303 K	-18.7622			22.31
318 K	-20.5212	15.85646	114.3009	23.4925
333 K	-22.1882			24.1925

Table 8 — Assessment of the maximum adsorption capacity of MG dye on different adsorbents

Adsorbent	q_m (mg g^{-1})	pH	Isotherm	Kinetic	References
Cellulose powder	2.42	7.2	FIM and LIM	PSO	[51]
Khat (*Catha edulis*) stem AC	5.62	10	FIM	PSO	[26]
Peanut stick AC	2.57	5	FIM and LIM	PSO	[52]
Neem sawdust	4.354	7.2	LIM		[53]
Chollera based biomass	18.4			PSO	[54]
Commercial-grade activated carbon	8.27	7	FIM	PSO	[55]
Acid-activated carbon	9.78	6	LIM		[56]
Arundo donax root carbon (ADRC)	9.35	5	LIM	PSO	[57]
De-oiled rice bran based activated carbon (DORBAC)	70.92	9	FIM	PSO	This study

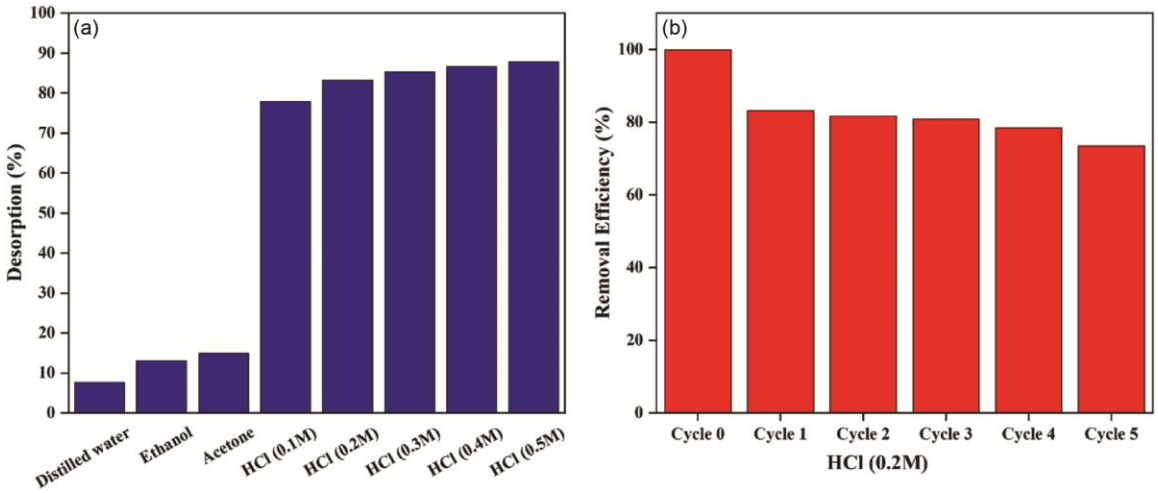

Fig. 6 — Regeneration and reusability of DORBAC: (a) desorption efficiency using different desorption agents and (b) reusability performance of the regenerated adsorbent over multiple cycles

conditions created by HCl, the adsorbent surface becomes protonated, reducing or neutralizing its negative charge. Weakened electrostatic attraction facilitates the release of malachite green from the surface, increasing desorption likelihood [59,60]. HCl concentrations between 0.1 M and 0.5 M were used for desorption studies. 0.2 M HCl solution is preferred for further desorption study as higher concentrations of HCl might degrade or alter the structure of the adsorbent material.

Fig. 6 (b) demonstrates the effectiveness of DORBAC in adsorbing 10 mg L^{-1} of MG following treated with 0.2 M of HCl to investigate its reusability. Predictably, the effectiveness of DORBAC in removing MG dye was reduced after five consecutive cycles, which can be ascribed to the reduction of active sites and partial pore blockage in DORBAC[61]. Partial desorption of MG at varying concentrations of HCl verified that suggests the possibility of chemisorption in the adsorption process.

Conclusion

Herein, AC derived from DORB was synthesized through a one-step H_3PO_4 activation method and evaluated for the elimination of MG dye from aqueous solutions. The synthesized adsorbent exhibited a large surface area (465 m^2 g^{-1}) and well-developed porous structure, contributing to its effective adsorption performance. Batch adsorption studies revealed that optimal removal was accomplished at pH 9, a defined adsorbent dosage of 0.4 g L^{-1}, and an equilibrium duration of 18 min. The adsorption process followed the FIM, indicating heterogeneous surface adsorption, while kinetic analysis showed better agreement with the pseudo-second-order model. The maximum adsorption capacity was found to be 70.92 mg g^{-1}. Thermodynamic analysis confirmed that the adsorption process is spontaneous, endothermic, and entropy driven. Regeneration studies demonstrated that DORBAC retains over 70% of its adsorption

efficiency after five cycles using 0.2 M HCl, indicating good reusability. Overall, DORBAC presents a low-cost, efficient, and sustainable adsorbent for the removal of MG dye, with potential applicability in wastewater treatment systems.

Acknowledgments

The authors extend their appreciation to the National Institute of Technology, Raipur for their ample facility offerings and steadfast support. The authors would also like to express their gratitude to the IITD CRF facility for generously providing lab facilities and support.

Conflict of interest

The authors declare no conflicts of interest.

References

1 Choudhary M, Kumar R & Neogi S, Activated biochar derived from Opuntia ficus-indica for the efficient adsorption of malachite green dye, Cu^{+2} and Ni^{+2} from water, *J Hazard Mater*, 392 (2020) 122441.

2 Raval N P, Shah P U & Shah N K, Malachite green "a cationic dye" and its removal from aqueous solution by adsorption, *Appl Water Sci*, 7 (2017) 3407.

3 Zhang C, Guo D, Shen T, Hou X, Zhu M, Liu S & H Q, Titanium dioxide/magnetic metal-organic framework preparation for organic pollutants removal from water under visible light, *Colloids Surf A Physicochem Eng Asp*, 589 (2020) 124484.

4 Hashimoto J C, Paschoal J A R, De Queiroz J F & Reyes F G R, Considerations on the use of malachite green in aquaculture and analytical aspects of determining the residues in fish: A review, *J Aquat Food Prod Technol*, 20 (2011) 273.

5 Panel E & Chain F, Malachite green in food, *EFSA J*, 14 (2016) 4530.

6 Nayeri D & Mousavi S A, Dye removal from water and wastewater by nanosized metal oxides - modified activated carbon: A review on recent researches, *J Environ Health Sci Eng*, 18 (2020) 1671.

7 Murthy T P K, Gowrishankar B S, Prabha M N C, Kruthi M & Krishna R H, Studies on batch adsorptive removal of malachite green from synthetic wastewater using acid treated coffee husk: Equilibrium, kinetics and thermodynamic studies, *Microchem J*, 146 (2019) 192.

8 Bello O S, Adegoke K A & Akinyunni O O, Preparation and characterization of a novel adsorbent from Moringa oleifera leaf, *Appl Water Sci*, 7 (2017) 1295.

9 Donya S M, Farghaly A A, Abo-Zeid M A, Aly H F, Ali S A, Hamed M A & El-Rigal N S, Malachite Green induces genotoxic effect and biochemical disturbances in mice, *Eur Rev Med Pharmacol Sci*, 16 (2012) 469.

10 Prates R A, Yamada A M, Suzuki L C, Hashimoto M C E, Cai S, Gouw-Soares S, Gomes L & Ribeiro M S, Bactericidal effect of malachite green and red laser on Actinobacillus actinomycetemcomitans, *J Photochem Photobiol B*, 86 (2007) 70.

11 Kim M, Sharma N, Chung J & Yun K, Activated graphene with fractal structure for the adsorption of malachite green with high removal rate, *Micropor Mesopor Mater*, 322 (2021) 111166.

12 Crini G, Non-conventional low-cost adsorbents for dye removal: A review, *Bioresour Technol*, 97 (2006) 1061.

13 Bello O S & Ahmad M A, Coconut (Cocos nucifera) shell based activated carbon for the removal of malachite green dye from aqueous solutions, *Sep Sci Technol*, 47 (2012) 903.

14 Kumar K A & Sandeep S, Adsorption kinetics of malachite green dye removal from aqueous solution by using banana stem, *Int J Eng Adv Technol*, 10 (2021) 215.

15 Pandey L K, Gaikwad M S & Chaudhari P K, Biowaste materials derived activated carbon (BMDAC) electrodes for removal of pollutant ions using capacitive deionization: A mini review, *Mater Lett*, 340 (2023) 134165.

16 Qamar O A, Jamil F, Hussain M, Al-Muhtaseb A H, Inayat A, Waris A, Akhter P & Park Y K, Feasibility-to-applications of value-added products from biomass: Current trends, challenges, and prospects, *Chem Eng J*, 454 (2023) 140240.

17 Kumar S, Sahu N P, Shamna N & Ranjan A, Feeding higher level of de-oiled rice bran causes stress to Labeorohita fingerlings, *Aquaculture*, 484 (2018) 184.

18 Zhao X, Hua Q, Wang C, Wang X, Zhang H, Zhang K, Zheng B, Yang J & Niu J, Study on adsorption performance and mechanism of peanut hull-derived magnetic biochar for removal of malachite green from water, *Mater Res Express*, 10 (2023) 095504.

19 Kumar K A & Sandeep S, Adsorption kinetics of malachite green dye removal from aqueous solution by using banana stem, *Int J Eng Adv Technol*, 10 (2021) 215.

20 Guo Y & Rockstraw D A, Activated carbons prepared from rice hull by one-step phosphoric acid activation, *Micropor Mesopor Mater*, 100 (2007) 12.

21 Chouli F, Ezzat A O, Sabantina L, Benyoucef A & Zehhaf A, Optimization conditions of malachite green adsorption onto almond shell carbon waste using process design, *Molecules*, 29 (2024) 54.

22 Dahri M K, Kooh M R R & Lim L B L, Water remediation using low cost adsorbent walnut shell for removal of malachite green: Equilibrium, kinetics, thermodynamic and regeneration studies, *J Environ Chem Eng*, 2 (2014) 1434.

23 Arfi R B, Karoui S, Mougin K & Ghorbal A, Adsorptive removal of cationic and anionic dyes from aqueous solution by utilizing almond shell as bioadsorbent, *Euro Mediterr J Environ Integr*, 2 (2017) 1.

24 Hameed B H & El-Khaiary M I, Kinetics and equilibrium studies of malachite green adsorption on rice straw-derived char, *J Hazard Mater*, 153 (2008) 701.

25 Li Y, Du Q, Liu T, Peng X, Wang J, Sun J, Wang Y, Wu S, Wang Z, Xia Y & Xia L, Comparative study of methylene blue dye adsorption onto activated carbon, graphene oxide, and carbon nanotubes, *Chem Eng Res Des*, 91 (2013) 361.

26 Abate G Y, Alene A N, Habte A T & Getahun D M, Adsorptive removal of malachite green dye from aqueous solution onto activated carbon of Catha edulis stem as a low cost bio-adsorbent, *Environ Syst Res*, 9 (2020) 29.

27 Kamalakkannan J, Chandraboss V L, Prabha S & Senthilvelan S, Advanced construction of heterostructured $InCrO_4$-TiO_2 and its dual properties of greater UV-photocatalytic and antibacterial activity, *RSC Adv*, 5 (2014) 77000.

28 Li Y M, Sun S Q, Zhou Q, Qin Z, Tao J X, Wang J & Fang X, Identification of American ginseng from different regions using FT-IR and two-dimensional correlation IR spectroscopy, *Vib Spectrosc*, 36 (2004) 227.

29 Samargandi D, Zhang X, Liu F & Tian S, Research article fourier transform infrared (FT-IR) spectroscopy for discrimination of fenugreek seeds from different producing areas, *J Chem Pharm Res*, 6 (2014) 19.

30 Kooh M R R, Lim L B L, Lim L H & Bandara J M R S, Batch adsorption studies on the removal of malachite green from water by chemically modified Azolla pinnata, *Desal Water Treat*, 57 (2016) 14632.

31 Bekçi Z, Özveri C, Seki Y & Yurdakoç K, Sorption of malachite green on chitosan bead, *J Hazard Mater*, 154 (2008) 254.

32 Karadeniz D, Kahya N & Erim F B, Effective photocatalytic degradation of malachite green dye by Fe(III)-cross-linked alginate-carboxymethyl cellulose composites, *J Photochem Photobiol A Chem*, 428 (2022) 113867.

33 Mashinchian O, Johari-Ahar M, Ghaemi B, Rashidi M, Barar J & Omidi Y, Impacts of quantum dots in molecular detection and bioimaging of cancer, *Bioimpacts*, 4 (2014) 149.

34 Jesurani S, Kanagesan S, Velmurugan R & Kalaivani T, Phase formation and high dielectric constant of calcium copper titanate using sol-gel route, *J Mater Sci: Mater Electron*, 23 (2012) 668.

35 Khan M A, Otero M, Kazi M, Alqadami A A, Wabaidur S M, Siddiqui M R, Alothman Z A & Sumbul S, Unary and binary adsorption studies of lead and malachite green onto a nanomagnetic copper ferrite/drumstick pod biomass composite, *J Hazard Mater*, 365 (2019) 759.

36 Manullang J R, Nugroho R A, Rohmah M, Rudianto R & Qorysuchi A, Plant-extract-mediated biosynthesis of silver nanoparticles using Eleutherine americana bulb extract and its characterization, *Nusantara Biosci*, 13 (2021) 247.

37 Panda J & Tudu B, Hydrothermally synthesized flower like MoS_2 microsphere: A highly efficient adsorbent for methylene blue dye removal, *AIP Conf Proc*, 1953 (2018) 030127.

38 Trikkaliotis D G, Mitropoulos A C & Kyzas G Z, Low-cost route for top-down synthesis of over- and low-oxidized graphene oxide, *Colloids Surf A Physicochem Eng Asp*, 600 (2020) 124928.

39 Niticharoenwong B, Shotipruk A, Mekasuwandumrong O, Panpranot J & Jongsomjit B, Characteristics of activated carbons derived from deoiled rice bran residues, *Chem Eng Commun*, 200 (2013) 1309.

40 Osman A I, Blewitt J, Abu-Dahrieh J K, Farrell C, Al-Muhtaseb A H, Harrison J & Rooney D W, Production and characterisation of activated carbon and carbon nanotubes from potato peel waste and their application in heavy metal removal, *Environ Sci Pollut Res*, 26 (2019) 37228.

41 Xiong C, Jia Q, Chen X, Wang G & Yao C, Optimization of polyacrylonitrile-2-aminothiazole resin synthesis, characterization, and its adsorption performance and mechanism for removal of Hg(II) from aqueous solutions, *Ind Eng Chem Res*, 52 (2013) 4978.

42 Muttakin M, Mitra S, Thu K, Ito K & Saha B B, Theoretical framework to evaluate minimum desorption temperature for IUPAC classified adsorption isotherms, *Int J Heat Mass Transf*, 122 (2018) 795.

43 Rawat A P & Singh D P, Decolourization of malachite green dye by mentha plant biochar (MPB): A combined action of adsorption and electrochemical reduction processes, *Water Sci Technol*, 77 (2018) 1734.

44 Ahmad R & Kumar R, Adsorption studies of hazardous malachite green onto treated ginger waste, *J Environ Manag*, 91 (2010) 1032.

45 Rashad E, Saleh H N, Eltaweil A S, Saleh M E, Sillanpaa M & Mostafa A R, Pinewood sawdust biochar as an effective biosorbent for PAHs removal from wastewater, *Biomass Convers Biorefin*, 13 (2023) 13443.

46 Chung H K, Kim W H, Park J, Cho J, Jeong T Y & Park P K, Application of Langmuir and Freundlich isotherms to predict adsorbate removal efficiency or required amount of adsorbent, *J Ind Eng Chem*, 28 (2015) 241.

47 Ajenifuja E, Ajao J A & Ajayi E O B, Adsorption isotherm studies of Cu (II) and Co (II) in high concentration aqueous solutions on photocatalytically modified diatomaceous ceramic adsorbents, *Appl Water Sci*, 7 (2017) 3793.

48 Ahmad M A, Ahmad N & Bello O S, Adsorptive removal of malachite green dye using durian seed-based activated carbon, *Water Air Soil Pollut*, 225 (2014) 2057.

49 Borsato D, Galvan D, Pereira J L, Orives J R, Angilelli K G & Coppo R L, Kinetic and thermodynamic parameters of biodiesel oxidation with synthetic antioxidants: Simplex centroid mixture design, *J Braz Chem Soc*, 25 (2014) 1984.

50 Chouli F, Ezzat A O, Sabantina L, Benyoucef A & Zehhaf A, Optimization conditions of malachite green adsorption onto almond shell carbon waste using process design, *Molecules*, 29 (2024) 54.

51 Sekhar C P, Kalidhasan S, Rajesh V & Rajesh N, Bio-polymer adsorbent for the removal of malachite green from aqueous solution, *Chemosphere*, 77 (2009) 842.

52 Ghaedi M, Nasab A G, Khodadoust S, Rajabi M & Azizian S, Application of activated carbon as adsorbents for efficient removal of methylene blue: Kinetics and equilibrium study, *J Ind Eng Chem*, 20 (2014) 2317.

53 Khattri S D & Singh M K, Removal of malachite green from dye wastewater using neem sawdust by adsorption, *J Hazard Mater*, 167 (2009) 1089.

54 Tsai W T & Chen H R, Removal of malachite green from aqueous solution using low-cost chlorella-based biomass, *J Hazard Mater*, 175 (2010) 844.

55 Mall I D, Srivastava V C, Agarwal N K & Mishra I M, Adsorptive removal of malachite green dye from aqueous solution by bagasse fly ash and activated carbon-kinetic study and equilibrium isotherm analyses, *Colloids Surf A Physicochem Eng Asp*, 264 (2005) 17.

56 Venkatraman B R, Rajachandrasekar T, Herna M & Arivoli S, Adsorption kinetics and thermodynamics of copper metal ion on to acid activated low cost carbon, *Indian J Environ Prot*, 27 (2007) 813.

57 Zhang J, Li Y, Zhang C & Jing Y, Adsorption of malachite green from aqueous solution onto carbon prepared from Arundo donax root, *J Hazard Mater*, 150 (2008) 774.

58 Vijayaraghavan K & Yun Y S, Bacterial biosorbents and biosorption, *Biotechnol Adv*, 26 (2008) 266.

59 Bouaziz F, Koubaa M, Kallel F, Ghorbel R E & Chaabouni S E, Adsorptive removal of malachite green from aqueous solutions by almond gum: Kinetic study and equilibrium isotherms, *Int J Biol Macromol*, 105 (2017) 56.

60 Baek M H, Ijagbemi C O, Se-Jin O & Kim D S, Removal of malachite green from aqueous solution using degreased coffee bean, *J Hazard Mater*, 176 (2010) 820.

61 Abewaa M, Mengistu A, Takele T, Fito J & Nkambule T, Adsorptive removal of malachite green dye from aqueous solution using Rumex abyssinicus derived activated carbon, *Sci Rep*, 13 (2023) 1.